ORIGINAL ARTICLE

lajss.org Latin American Journal of Solids and Structures

www.lajss.org

Robust Adaptive Control for Micro-Vibration Suppression under Multiple Unknown Narrow-Band Disturbances

Fang Yubin[a], Liang Chaojun[a], Tian Mengchu[b*]

[a]School of Mechanical Engineering, Jiangsu University of Technology, Changzhou 213001, China. E-mails: fangyubin91@163.com, 2023655159@smail.jstu.edu.cn.
[b]Nanjing University of Science and Technology, Nanjing 210094, China. E-mail: tianmengchu@njust.edu.cn.

*Corresponding author

https://doi.org/10.1590/1679-7825/e8782

Abstract

While the Youla–Kučera (Y–K) parameterization can suppress unknown and time-varying narrow-band disturbances, its performance depends heavily on an accurate secondary-path model, which is often difficult or impossible to obtain in practice. To address this limitation, this work proposes a direct feedback robust adaptive micro-vibration control algorithm that does not rely on secondary-path identification. The controller integrates the Y–K framework with a variable step-size LMS (VSSLMS) scheme for real-time parameter adaptation, ensuring closed-loop stability while improving convergence and robustness under multi-frequency time-varying disturbances. Experiments on an active micro-vibration platform show that the proposed method achieves over 60% improvement in steady-state suppression compared with conventional FxLMS and Y–K + LMS algorithms, particularly under dual-frequency disturbances with spectrum and amplitude variations. These results demonstrate that the method provides a model-independent and robust solution for micro-vibration suppression in precision satellite systems.

Keywords

Micro-vibration control, Robust adaptive, Variable step size (VSS), Y-K parameterization, Least mean square

Graphical abstract

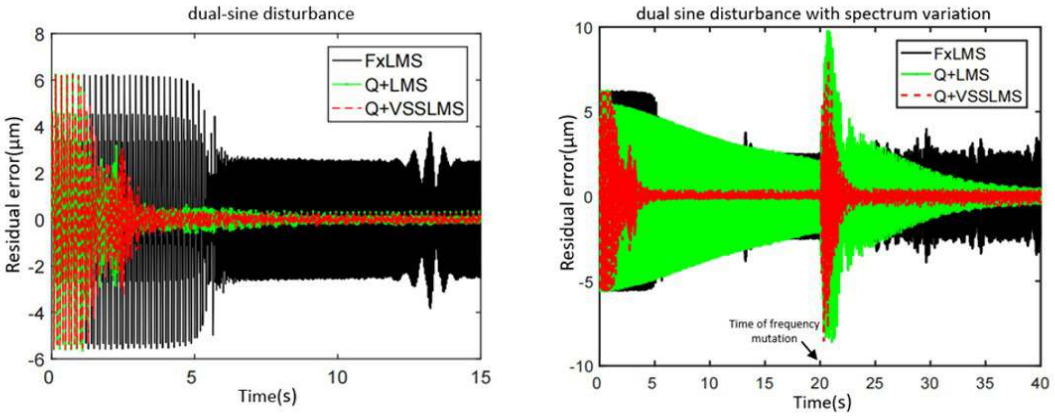

Received July 29, 2025. In revised form October 21, 2025. Accepted November 12, 2025. Available online November 14, 2025.
https://doi.org/10.1590/1679-7825/e8782

Latin American Journal of Solids and Structures. ISSN 1679-7825. Copyright © 2026. This is an Open Access article distributed under the terms of the Creative Commons Attribution License, which permits unrestricted use, distribution, and reproduction in any medium, provided the original work is properly cited.

1 INTRODUCTION

When a satellite operates in space, it is subjected to disturbances from the space environment as well as its own rotating parts. These disturbances induce micro-vibrations in the structure, often characterized by multiple frequency bands (LEE D-O et al., 2016). In the case of high-resolution satellites equipped with precise optical payloads, these micro-vibrations can lead to optical axis jitter and image motion, ultimately resulting in a reduction in image resolution (LI L et al., 2021). Consequently, their impact cannot be underestimated. Hence, the suppression of micro-vibrations within satellite structures has emerged as a crucial research area and a prominent topic of interest among scholars (MENG G et al., 2015).

Currently, active control or a combination of active and passive control are often used to suppress structural micro-vibrations. Regarding active control methods, current research covers most of the content in control theory (WANG L et al., 2020; SUN Y et al., 2018). From the control-theory perspective, achieving effective disturbance suppression requires that the controller incorporate a disturbance model (LANDAU I D, 2020). Therefore, the disturbance model must be embedded in the closed-loop controller during the design stage.Thus, the micro-vibration response caused by the disturbance is counteracted under the premise of stable closed-loop system (WANG J et al., 2017). Because the space disturbance environment is complex and often time-varying, its characteristics are typically unknown, which affects the control performance of satellite micro-vibration systems. In this case, adaptive control methods have obvious advantages.

As a useful tool in adaptive control field, The Youla–Kučera (Y–K) parameterization method was independently proposed by Youla and Kučera in the 1970s. It provides a family of stable linear controllers for linear time-invariant plants in feedback systems through the cooperation between an adaptive filter and a central robust controller (YOULA D et al., 1976a; YOULA D et al., 1976b). The advantage of this method is that the parameter estimation of the internal mode of the disturbance can be implemented without changing the closed-loop poles of control system. In the 1990s, the development of the Y-K parameterization method and its applications in system identification, adaptive control, and nonlinear systems was systematically described (ANDERSON B D O, 1998). In the following 20 years, Y-K parameterization method was gradually introduced into the field of active vibration & noise control (AVNC), and achieved satisfactory control performance (LANDAU I D, 2020).

Currently, the Y-K parameterization method is employed to address two primary challenges in AVNC. The first challenge revolves around mitigating the positive feedback effect in feedforward AVNC systems. In a feedforward AVNC system, the reference signal is influenced by the actuator's output. Thus, a positive feedback loop is formed. The presence of positive feedback loop makes the original control system no longer a pure feedforward system, which affects the stability of the system. The Y-K parameterization method was first used for the positive feedback effect problem in feedforward vibration active control (AVC) system and achieved a better control effect (LANDAU I D, 2010). Subsequently, Landau's team did a lot of meaningful work on this issue including the application of different forms of filters, different adaptive parameters, different filtering algorithms. The applicability and superiority of Y-K parameterization method for the stability problems with feedforward system caused by positive feedback loop is demonstrated through stability analysis and experimental verification (LANDAU I D et al., 2020; LANDAU I D et al., 2010; LANDAU I D et al., 2011a; LANDAU I D et al., 2012; LANDAU I D et al., 2013; TUDOR-BOGDAN AIRIMITOAIE I D L et al., 2013; LANDAU I D et al., 2019a; LANDAU I D et al., 2019b; LANDAU I D et al., 2021).

The suppression of multi-frequency time-varying and unknown narrowband disturbance is another fundamental issue in the field of ANVC (LANDAU I D et al., 2011b). The feedback control system has a good suppression effect for narrow band disturbance while its control effect is limited by the Bode integral of the output sensitivity function and ‘waterbed’ effect. At this moment, it is usually used by cooperating with feedforward control system or by establishing internal model of the disturbance (SILVA A C et al., 2013). However, it is difficult to obtain or even find the disturbance source in many applications for placing a reference sensor. The problem of internal model establishment of the disturbance is solved by Y-K parameterization method successfully without changing the poles of the system. It achieves better control results in suppression with unknown and time-varying multi-frequency narrow-band disturbances (WANG J et al., 2017; LANDAU I D et al., 2016; CHEN X et al., 2015; LANDAU I D et al., 2015; VAU B et al., 2021). As far as the feedback adaptive control method based on Y-K parameterization is concerned, most of the current research design parameters of the central robust controller with a known mathematical model of the secondary path. For example, pole placement method (LANDAU I D et al., 2015; AIRIMITOAIE T-B et al., 2018), H-infinity (QIAN F F et al., 2019), and optimal control method (WU Z et al., 2019) were used.

In recent years, several studies have extended the Y–K parameterization method toward more challenging scenarios with uncertain or unknown secondary paths. Regarding the problem of suppressing unknown tilt disturbances in image stabilization systems, an adaptive Y-K scheme has been proposed and applied in previous studies (Ruan et al. 2022), which further validates the applicability of this framework to optical platforms.Subsequent research explored

combinations of Y–K with robust controller synthesis; for instance, an LQG/LTR-based Youla parameterized adaptive controller was proposed (HAICHUN D et al,2024) to enhance robustness under plant uncertainties.

In addition to control-oriented extensions of the Y–K framework, recent studies have also explored mechanical-inertia and aerodynamic actuation strategies that provide complementary approaches to active vibration suppression. For flexible pendulum systems, a planned-flywheel motion strategy was developed to increase equivalent damping and thereby suppress large-amplitude vibration, supported by both theoretical analysis and experiments(Ruan Y. et al. 2023). Furthermore, the flywheel-assembly concept has been applied to three-dimensional flexible beams, demonstrating that coordinated inertial actuation can achieve broadband vibration attenuation in multiple axes(Zhang L. et al. 2024). In a related class of problems, aerodynamic-force based actuation has been shown effective for suppressing oscillations of suspended loads with compact devices and modest force requirements, offering a practical non-contact solution for constrained environments(Chu W. & Wang Y.Q. 2025). These works complement the present study by showing alternative actuation paradigms (inertia or aerodynamic force) that can be combined with or used instead of piezoelectric feedback schemes in specific application scenarios.

However, the design of a central robust controller requires an accurate mathematical model of the secondary path in satellite, which puts forward corresponding precision requirements for system identification. Moreover, there are also some instances where the model of the secondary path is unknown. In such cases, the control effect of the central robust controller based on a model may weaken or even fail.

This paper addresses the challenge of active control of multi-frequency time-varying or unknown narrowband disturbances when an accurate model of the secondary path cannot be obtained. To overcome this challenge, an active micro-vibration control experimental system is constructed for implementing an adaptive control algorithm. Taking the advantages of the Y-K parameterization method in active vibration control, this paper proposes a feedback adaptive control algorithm with PID method as the central robust controller to cope with multi-frequency narrow-band disturbances when the secondary path model is not easy to obtain. At the same time, a new variable step size least mean square (VSSLMS) method is proposed as the parameter adaptive algorithm (PAA) to get a better convergence effect. Finally, the vibration suppression effect of the proposed feedback adaptive control algorithm is verified through real-time experiments.

Although this study focuses on satellite structures, the proposed control framework is generic and can be applied to other precision systems where micro-vibrations degrade performance, such as optical benches, lithography stages, and nano-positioning platforms.

2 Experimental system

To validate the efficacy of the AVC algorithm, a nano-positioning unit based piezoelectric stacks is used. This unit was designed to replicate disturbances and actively suppress micro-vibrations along the x, y, and z axes. Figure 1 depicts an illustration of the aforementioned unit, comprising several components: a baseplate, a vibration excitation module, a vibration suppression module, a working stage, and three displacement sensors.

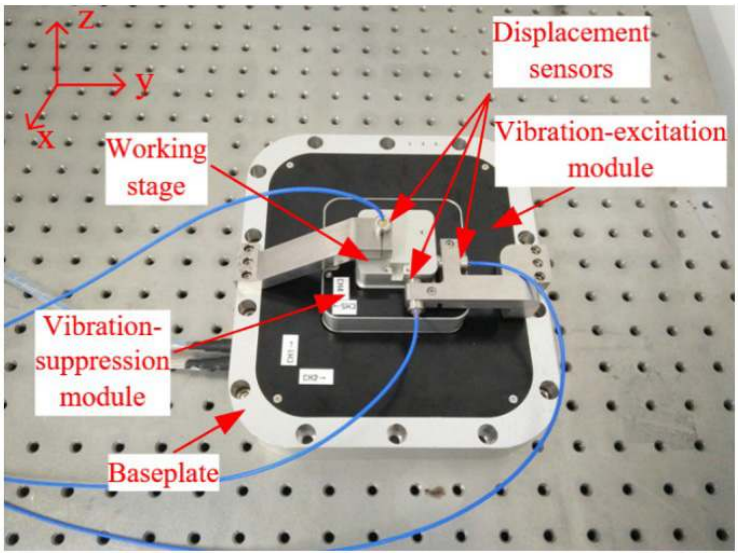

Figure 1 *Schematic representation of the nano-positioning unit*

Functional modules and components of the nano-positioning unit:

a. Baseplate securely mounted on an optical vibration isolation platform to shield the nano-position unit from external disturbances.

b. Vibration excitation module designed for emulating external micro-vibration disturbances.

c. Vibration suppression module equipped to counteract micro-vibrations using the control algorithm.

d. Displacement sensors employed to collect vibration error data.

e. Working stage, with the goal of achieving vibration suppression.

In the AVC experimental setup, the excitation device and the vibration-control actuator are integrated within the nano-positioning unit. The excitation device consists of a piezoelectric stack actuator, which generates precise micro-vibrations by applying a controlled voltage signal. This actuator serves a dual role: it introduces external disturbances to simulate unwanted vibrations and also functions as the vibration-control actuator to counteract these disturbances under active control. The flexible hinge mechanism ensures single-axis motion while minimizing mechanical cross-coupling, and the displacement sensor (capacitive or strain-gauge type) continuously measures the platform's position and vibration amplitude.

The sensor signal is conditioned and transmitted to the data acquisition board (NI PCI-6289) installed on the target PC, where real-time computation of the control algorithm is performed through the MATLAB xPC Target environment. The resulting control output is amplified and fed back to the piezoelectric actuator to achieve active vibration suppression. The host PC communicates with the target PC to monitor the experiment and adjust control parameters in real time.

The overall workflow of signal transmission and control implementation is illustrated in Figure 2, which presents the flow diagram of the AVC experimental system based on the nano-positioning unit. The system comprises two industrial control computers (ACP-4020, Advantech©) interconnected in real-time with the MATLAB© xPC Target environment (R2016b). Among the computers, one functions as the target PC, while the other operates as the host PC. The target PC is outfitted with a pair of data acquisition boards (PCI-6289, NI©) responsible for both data collection and control output. Figure 3 captures a visual representation of the AVC experimental system.

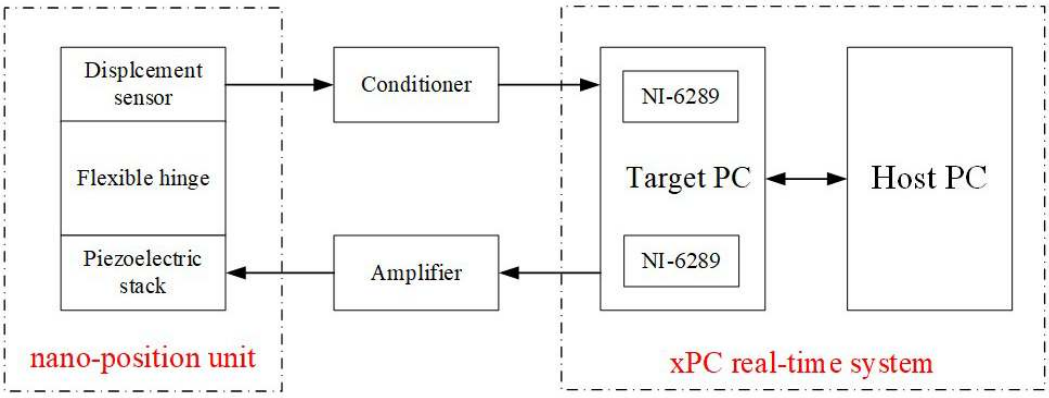

Figure 2 *Structural diagram of the AVC experimental system based on the nano-position unit*

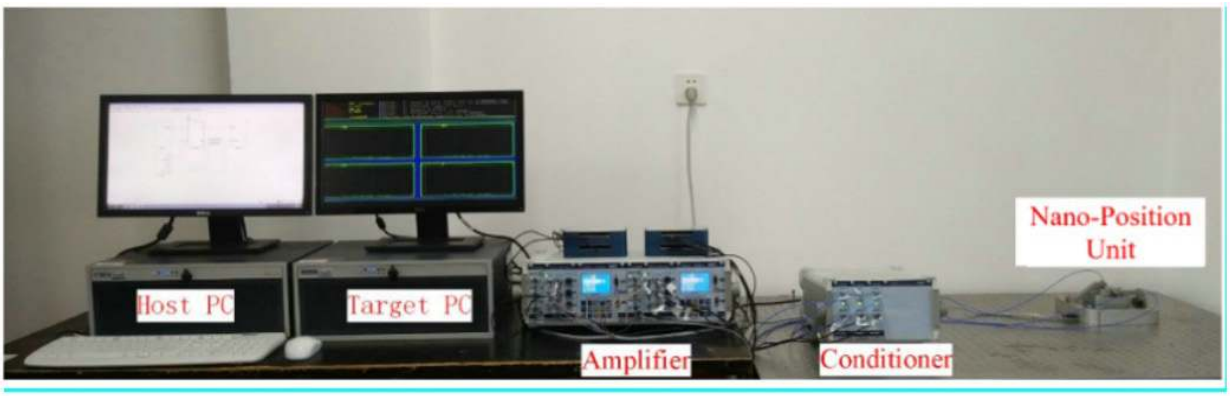

Figure 3 *Image of the AVC experimental system*

3 Feedback AVC algorithm based on Y-K parameterization method

Although the Y–K parameterization framework has been extensively studied in adaptive feedforward vibration control, most previous works rely on a known or accurately identified secondary path model to design the central robust controller through pole placement, $H\infty$, or optimal control techniques.

In contrast, the approach proposed in this study eliminates the dependency on an explicitly identified secondary path. Instead of embedding the plant model into controller synthesis, a direct feedback configuration is established, where the Y–K parameterization filter is adaptively tuned using only the measured residual error. This structure enables real-time adjustment of controller parameters while maintaining closed-loop pole invariance guaranteed by the Y–K formulation. Consequently, the proposed framework achieves robust vibration suppression even when the secondary path is uncertain, time-varying, or difficult to model accurately.

The robustness of the proposed controller arises from the Y–K parameterization framework, where the adaptive filter operates without altering the closed-loop poles fixed by the central robust controller. Thus, stability is preserved under modeling errors or secondary-path variations. Meanwhile, adaptivity is ensured by the variable step-size LMS algorithm, which dynamically adjusts filter coefficients based on the measured vibration error, enabling fast convergence and effective tracking of multi-frequency time-varying disturbances. Together, these two features allow the controller to maintain stable and efficient vibration suppression across varying operating conditions.

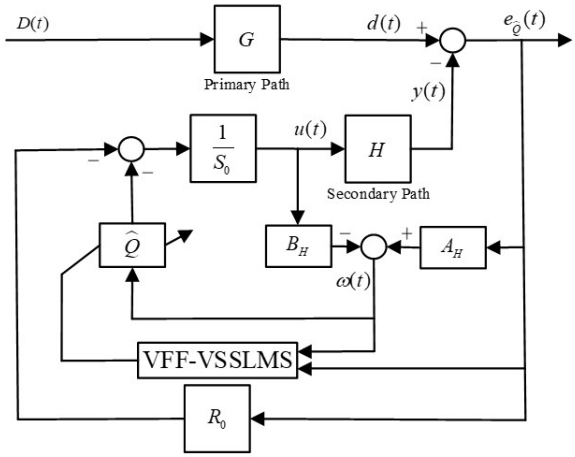

Figure 4 *Block diagram of the feedback Youla-Kucera adaptive control algorithm*

Figure 4 depicts the block diagram of the feedback AVC algorithm based on Y-K parameterization given in this paper. Equation (1) and (2) respectively represent G and H , which denote the primary path and secondary path of the system.

$$G(q^{-1})=\frac{q^{-d_G}B_G(q^{-1})}{A_G(q^{-1})} \tag{1}$$

$$H(q^{-1})=\frac{q^{-d_H}B_H(q^{-1})}{A_H(q^{-1})} \tag{2}$$

$$A_G(q^{-1}) = I + a_1^G q^{-1} + a_2^G q^{-2} + \cdots + a_{n_{AG}}^G q^{-n_{AG}} \tag{3}$$

$$B_G(q^{-1}) = b_1^G q^{-1} + b_2^G q^{-2} + \cdots + b_{n_{BG}}^G q^{-n_{BG}} \tag{4}$$

$$A_H(q^{-1}) = I + a_1^H q^{-1} + a_2^H q^{-2} + \cdots + a_{n_{AH}}^H q^{-n_{AH}} \tag{5}$$

$$B_H(q^{-1}) = b_1^H q^{-1} + b_2^H q^{-2} + \cdots + b_{n_{BH}}^H q^{-n_{BH}} \tag{6}$$

In Equations (1) and (2), d_G and d_H respectively denote the integer delays of the primary path and secondary path. $d(t)$ represents the micro-vibration response of the primary path when excited by disturbance $D(t)$ (a known model structure), while $y(t)$ denotes the micro-vibration response of the secondary path. The system residual signal is represented as $e(t)$. $\widehat{A}_G(q^{-1})$, $\widehat{B}_G(q^{-1})$, $\widehat{A}_H(q^{-1})$ and $\widehat{B}_H(q^{-1})$ are used to represent the estimated values of $A_G(q^{-1})$, $B_G(q^{-1})$, $A_H(q^{-1})$ and $B_H(q^{-1})$. In this paper, it is assumed that the accurate model of $A_G(q^{-1})$, $B_G(q^{-1})$, $A_H(q^{-1})$ and $B_H(q^{-1})$ can be obtained through system identification. It means $\widehat{A}_G(q^{-1}) = A_G(q^{-1})$, $\widehat{B}_G(q^{-1}) = B_G(q^{-1})$, $\widehat{A}_H(q^{-1}) = A_H(q^{-1})$, $\widehat{B}_H(q^{-1}) = B_H(q^{-1})$. Within the feedback control system illustrated in Figure 4, the central robust controller designed by the PID method, composed of polynomials $R_0(q^{-1})$ and $S_0(q^{-1})$, is denoted as $N_0(q^{-1})$. Details are given in Equations (7) to (9).

$$N_0(q^{-1}) = \frac{R_0(q^{-1})}{S_0(q^{-1})} \tag{7}$$

$$S_0(q^{-1}) = I + s_1^0 q^{-1} + s_2^0 q^{-2} + \cdots + s_{n_{S0}}^0 q^{-n_{S0}} \tag{8}$$

$$R_0(q^{-1}) = r_1^0 + r_2^0 q^{-1} + \cdots + r_{n_{R0}}^0 q^{-n_{R0}} \tag{9}$$

Equations (10) to (11) display the input $e(t)$ and output $u(t)$ of the feedback controller when the central robust controller is used in isolation.

$$e(t) = d(t) - \frac{q^{-d_H} B_H(q^{-1})}{A_H(q^{-1})} \cdot u(t) \tag{10}$$

$$S_0(q^{-1}) \cdot u(t) = -R_0(q^{-1}) \cdot e(t) \tag{11}$$

As presented in Equation (12), the closed-loop pole distribution of the system is determined by the characteristic polynomial $P_0(q^{-1})$.

$$P_0(q^{-1}) = A_H(q^{-1}) S_0(q^{-1}) + q^{-d_H} B_H(q^{-1}) R_0(q^{-1}) \tag{12}$$

As presented in equation (13), when the Y-K parameterization filter is introduced into the feedback system, the input signal to $Q(q^{-1})$ is $\omega(t)$.

$$\omega(t) = A_H(q^{-1}) e(t) - q^{-d_H} B_H(q^{-1}) u(t) \tag{13}$$

Equation (14) displays the optimal value of $Q(q^{-1})$ for the Y-K parameterization filter in FIR form.

$$Q(q^{-1}) = Q_0 + Q_1 q^{-1} + Q_2 q^{-2} + \cdots + Q_{n_{BQ}} q^{-n_{BQ}} \tag{14}$$

At this stage, $Q(q^{-1})$ and the central robust controller $N_0(q^{-1})$ combine to create a new feedback robust adaptive controller $K(q^{-1})$, as presented in Equation (15).

$$K(q^{-1}) = \frac{R(q^{-1})}{S(q^{-1})} \tag{15}$$

Among them,

$$R(q^{-1}) = R_0(q^{-1}) + A_H(q^{-1})Q(q^{-1}) \tag{16}$$

$$S(q^{-1}) = S_0(q^{-1}) - q^{-d_H} B_H(q^{-1})Q(q^{-1}) \tag{17}$$

Equation (18) displays the characteristic polynomial $P(q^{-1})$ of the new closed-loop system.

$$P(q^{-1}) = A_H(q^{-1})S_0(q^{-1}) + q^{-d_H} B_H(q^{-1})R_0(q^{-1}) \tag{18}$$

It can be observed that the closed-loop pole distribution remains unchanged with the addition of the Y-K parameterization filter $Q(q^{-1})$.

Equation (19) represents the real-time system error between the actual vibration response and its estimated counterpart. Intuitively, minimizing this error allows the adaptive controller to continuously adjust the filter coefficients to match the unknown disturbance dynamics.

$$e(t) = \frac{S_0(q^{-1}) - q^{-d_H} B_H(q^{-1})Q(q^{-1})}{P(q^{-1})} \cdot \omega(t) \tag{19}$$

In the actual system, the model of system identification deviates from the actual system. Therefore, it is necessary to adjust the Y-K parameterization filter with a PAA to match the real-time disturbance model. Through the implementation of the PAA, the parameter estimate $\widehat{Q}(t, q^{-1})$ replaces $Q(q^{-1})$, as shown in Equation (20).

$$\widehat{Q}(t, q^{-1}) = \widehat{Q}_0(t) + \widehat{Q}_1(t)q^{-1} + \widehat{Q}_2(t)q^{-2} + \cdots + \widehat{Q}_{n_{BQ}}(t)q^{-n_{BQ}} \tag{20}$$

Equation (21) depicts the feedback robust adaptive controller.

$$\widehat{K}(t, q^{-1}) = \frac{R_0(q^{-1}) + A_H(q^{-1})\widehat{Q}(t, q^{-1})}{S_0(q^{-1}) - B_H(q^{-1})\widehat{Q}(t, q^{-1})} \tag{21}$$

The Equation (22) defines the adaptive error of the system.

$$\varepsilon(t) = e_{\widehat{Q}}(t) - e(t) \tag{22}$$

$e_{\widehat{Q}}(t)$ denotes the error signal obtained based on the filter estimates $\widehat{Q}(q^{-1})$ in the parameter adaptation process, as depicted in equation (23).

$$e_{\widehat{Q}}(t) = \frac{S_0(q^{-1}) - q^{-d_H} B_H(q^{-1})\widehat{Q}(t, q^{-1})}{P(q^{-1})} \cdot \omega(t) \tag{23}$$

Equation (19) and (23) are incorporated into Equation (22) to derive the adaptive error of the system.

$$\varepsilon(t) = [Q(q^{-1}) - \widehat{Q}(t, q^{-1})]\frac{q^{-d_H} B_H(q^{-1})}{P(q^{-1})}\omega(t) \tag{24}$$

Construct parameter vectors as shown in Equations (25) and (26).

$$\boldsymbol{Q} = [Q_0, Q_1 \cdots Q_{n_{BQ}}] \tag{25}$$

$$\widehat{\boldsymbol{Q}}(t)=[\widehat{Q}_0(t),\widehat{Q}_1(t)\cdots\widehat{Q}_{n_{BQ}}(t)] \tag{26}$$

Construct the system observation vector as shown in Equations (27) and (28).

$$\boldsymbol{\Phi}(t)=[1,\omega(t),\omega(t-1)\cdots\omega(t-n_{BQ}+1)] \tag{27}$$

$$\boldsymbol{\Phi}^*(t)=[1,\omega_1(t),\omega_1(t-1)\cdots\omega_1(t-n_{BQ}+1)] \tag{28}$$

In the above equations,

$$\omega_1(t)=\frac{q^{-d_H}B_H}{P_0}\omega(t) \tag{29}$$

Thus, the system adaptive error can be formulated as follows:

$$\varepsilon(t)=[\boldsymbol{Q}^T-\widehat{\boldsymbol{Q}}^T(t)]\boldsymbol{\Phi}^*(t) \tag{30}$$

Because the system perturbation is unknown, the optimal parameter vector $\boldsymbol{Q}$ is also uncertain. In order to find the parameter vector estimate $\widehat{\boldsymbol{Q}}(t)$ that is closest to $\boldsymbol{Q}$, it can be translated into finding a $\widehat{\boldsymbol{Q}}(t)$ that minimizes the cost function shown in equation (31):

Since the system perturbation remains unknown, the optimal parameter vector, denoted as $\boldsymbol{\theta}$, is likewise uncertain. To determine the parameter vector estimate, denoted as $\hat{\boldsymbol{\theta}}$, that best approximates $\boldsymbol{\theta}$, the problem can be reframed as seeking a $\hat{\boldsymbol{\theta}}$ that minimizes the cost function as described in equation (31):

$$J(\widehat{\boldsymbol{Q}},t)=\varepsilon^2(t) \tag{31}$$

The gradient of the squared instantaneous error of the system, specifically the Least Mean Square (LMS) algorithm, has been chosen as the parameter adaptive algorithm.

$$\nabla\varepsilon^2(t)=\frac{\partial\varepsilon^2(t)}{\partial\widehat{\boldsymbol{Q}}(t)}=-2\varepsilon(t)\boldsymbol{\Phi}^*(t) \tag{32}$$

The parameter update iteration for $\widehat{\boldsymbol{Q}}(t)$ can be obtained as shown in Equation (33). Equation (33) shows that the controller parameters are updated proportionally to the instantaneous error and input correlation, meaning that the algorithm self-adjusts to suppress vibration more effectively as the system learns the disturbance characteristics.

$$\begin{aligned}\widehat{\boldsymbol{Q}}(t+1)&=\widehat{\boldsymbol{Q}}(t)-\frac{\mu}{2}\nabla\varepsilon^2(\widehat{\boldsymbol{Q}},t)\\&=\widehat{\boldsymbol{Q}}(t)+\mu\varepsilon(t)\boldsymbol{W}^*(t)\end{aligned} \tag{33}$$

When the Y-K parameter filter is set to its optimal value, the system error becomes zero. Consequently, the system adaptive error $\varepsilon(t)$ can be replaced by the real-time error value $e_{\hat{Q}}(t)$, which is measured by the sensor in the actual system. Therefore, Equation (33) can be expressed as:

$$\widehat{\boldsymbol{Q}}(t+1)=\widehat{\boldsymbol{Q}}(t)+\mu e_{\hat{Q}}(t)\boldsymbol{\Phi}^*(t) \tag{34}$$

In Equation (34), μ is the step size factor for the iteration of the adaptive parameter matrix.

In summary, the expression of the feedback AVC control algorithm is presented in Equations (35) to (37).

$$u(t)=\frac{R_0(q^{-1})+A_H(q^{-1})\widehat{\boldsymbol{Q}}(t,q^{-1})}{S_0(q^{-1})-B_H(q^{-1})\widehat{\boldsymbol{Q}}(t,q^{-1})}e_{\hat{Q}}(t) \tag{35}$$

$$e_{\hat{Q}}(t)=\frac{S_0(q^{-1})-q^{-d_H}B_H(q^{-1})\widehat{\boldsymbol{Q}}(t,q^{-1})}{P(q^{-1})}\cdot\omega(t) \tag{36}$$

$$\widehat{\boldsymbol{Q}}(t+1)=\widehat{\boldsymbol{Q}}(t)+\mu e_{\hat{Q}}(t)\boldsymbol{\Phi}^{*}(t) \tag{37}$$

The LMS algorithm, a commonly used parametric adaptive algorithm, offers the advantage of simplicity and robustness. However, the presence of its fixed step factor creates a trade-off between con

After the introduction of the VSSLMS algorithm concept, scholars have proposed various forms of VSSLMS algorithms to enhance algorithm performance by adjusting the step size in real-time. One approach in VSSLMS algorithm involves adjusting the real-time step size by setting the forgetting factor to achieve improved convergence effects, as demonstrated by SILVA A C et al., (2013), CHEN X et al., (2015), and LANDAU I D et al., (2015). Furthermore, we have introduced an enhanced version of the VSSLMS algorithm based on previous work (LANDAU I D et al., 2011b), and the corresponding step update formulas are presented in Table 1.

Table 1. Summary and complexity of four VSSLMS algorithms

Algorithms	Step Size update formulas	Parameters
VSSLMS-A (KWONG R H et al., 1992)	$\mu(n)=\xi\mu(n-1)+\eta e^2(n-1)$	2(ξ , η)
VSSLMS-B (ABOULNASR T et al., 1995)	$\mu(n)=\xi\mu(n-1)+\eta p^2(n-1)$ $p(n)=\lambda p(n-1)+(1-\lambda)e(n)e(n-1)$	3(ξ , η , λ)
VSSLMS-C (HUANG B et al., 2015)	$\mu(n)=\xi\mu(n-1)+\eta e^2(n-1)e^2(n-2)$	2(ξ , η)
VSSLMS-D (FANG Y B et al., 2019)	$\mu(n)=\xi\mu(n-1)+\eta(n)e^2(n-1)$ $\eta(n)=\beta\cdot\operatorname{arccot}(\lvert e(n)\rvert)$	2(ξ , β)

In Table 1, for convenience, VSSLMS-A, VSSLMS-B, VSSLMS-C, and VSSLMS-D are used to represent the four aforementioned VSSLMS algorithms, respectively. While VSSLMS-D has yielded more significant enhancements when compared to other VSSLMS algorithms of the same type (VAU B et al., 2021), it's worth noting that the fixed value of the forgetting factor still adversely affects the convergence rate of the algorithm. To address the issues, the authors have introduced a variable forgetting factor enhancement method. By decaying the forgetting factor according to a specific curve, the algorithm's convergence speed is improved while maintaining the steady-state performance of the original algorithm. The forgetting factor update formulas are provided in Equations (38) and (39).

$$\xi(t)=\lambda_1(0)+1-\lambda_1(t) \tag{38}$$

$$\lambda_1(t)=\lambda_0\lambda_1(t-1)+1-\lambda_0 \tag{39}$$

In Equations (38) and (39), $\xi(t)$ denotes the variable forgetting factor. The parameters λ_0 and λ_1 are utilized to control the rate of decay. λ_0 takes values within the range 0 < λ_0 < 1, and its value is typically close to 1, such as $\lambda_0=0.90,...0.99$ .The value of λ_0 determines the decay rate of $\lambda_1(t)$. The closer the value of λ_0 is to 1, the slower the decay rate of parameter $\lambda_1(t)$. The decay curves of several classical values are depicted in Figure 5. $\lambda_1(0)$ represents the initial value of parameter $\lambda_1(t)$, and $\xi(t)$ decays from 1 to $\lambda_1(0)$.

The essence of adaptive control is parameter identification, and the convergence effect of this improved VSSLMS algorithm is verified through parameter identification experiments. It is assumed that the finite-dimensional adaptive

filter can exactly represent the real system (without model error). White noise signals are used to excite both the unknown system and the adaptive filter, and the system error is obtained from the output of the real system and the output of the model based on the measured noise. The system error reflects the deviation between the adaptive filter model and the real system. The mathematical model of the real system is represented as $W_{opt}^{T}=[0.5,\ 1.1,\ 0.8,\ 0.7,\ 0.6,\ 0.5,\ 0.4,\ 0.3,\ 0.2,\ 0.1]$, while measurement noise with a signal-to-noise ratio of 10 dB is applied, with the signal-to-noise ratio calculated according to $\mathrm{SNR}=10\lg(E(x^2(n))/E(v^2(n)))$.

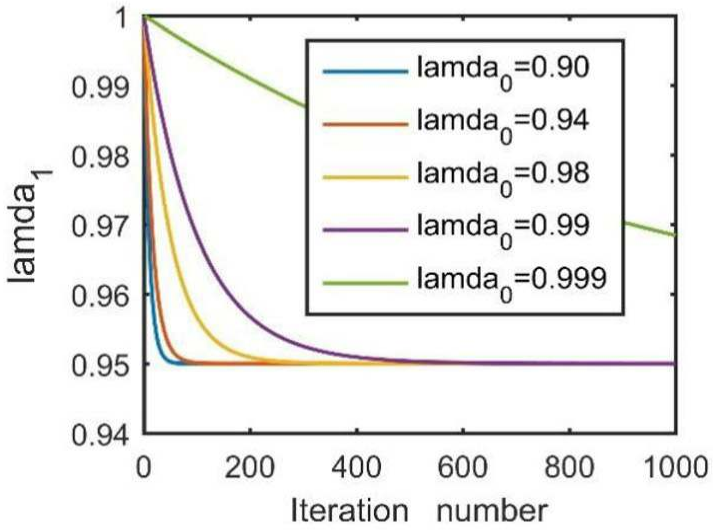

Figure 5 *Attenuation amplitude of* λ_1 *under classic value of* λ_0

Figure 5 illustrates how different values of the decay parameter β influence the evolution of the forgetting factor $\lambda(k)$. A larger β produces a slower decay, allowing the algorithm to retain more memory of past samples and thus improving steady-state stability but at the cost of slower adaptation to sudden spectral changes. Conversely, a smaller β yields a faster decay, enabling rapid adjustment of the adaptive filter to new disturbance conditions but potentially increasing transient fluctuations.

This dynamic trade-off between adaptation *speed* and steady-state accuracy is central to the proposed variable forgetting-factor mechanism. By shaping the decay profile of $\lambda(k)$, the algorithm can automatically balance convergence rate and robustness, maintaining high tracking performance even when the disturbance spectra or amplitudes vary abruptly.

Different VSSLMS algorithms mainly vary in how they update the step size. Intuitively, an adaptive step size enables faster convergence during large disturbances and smoother steady-state behavior when the system reaches equilibrium.

The acceleration effect of the variable forgetting factor can be theoretically interpreted through the adaptive law update in Eq. (40)–(44). When the forgetting factor $\lambda(k)$ decreases over time, the effective learning rate of recent error samples is proportionally increased, allowing the adaptive filter to respond more rapidly to new disturbance information. In the context of the mean-square convergence analysis of LMS-type algorithms, a smaller $\lambda(k)$ reduces the bias of recent gradient estimates and enhances tracking ability under nonstationary environments. Therefore, the gradual decay of $\lambda(k)$ provides a mechanism for dynamic adjustment of the equivalent step size, achieving faster transient convergence while preserving steady-state stability.

Parameter identification simulations were performed for the above four VSSLMS algorithms based on the improved form of the forgetting factor. For parameter identification, the combination of parameters recommended by the authors in the original literature was used. The value of parameter $\lambda_1(0)$ is the same as the forgetting factor ξ in the original literature, and other parameters such as upper and lower limits remain consistent with the original literature. To ensure that the four algorithms have the same initial convergence speed, they were set to have the same initial step size. After

several experiments, the Mean Squared Error (MSE) was used as the performance comparison metric for each algorithm, as depicted in Figure 6.

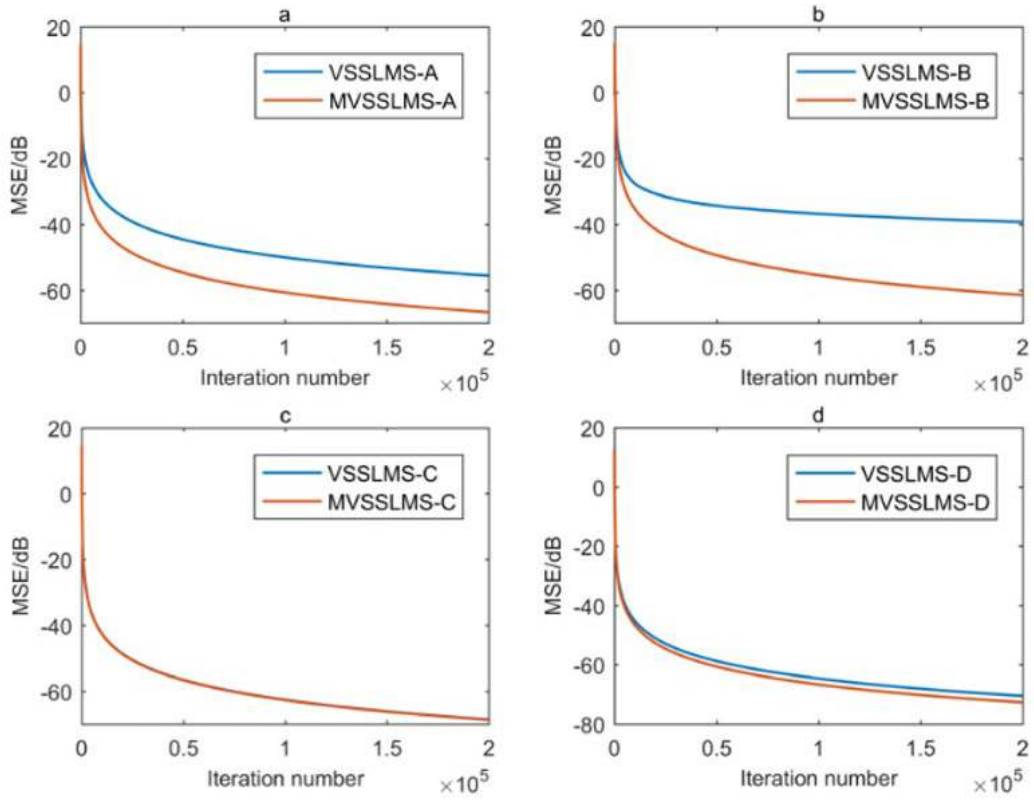

Figure 6 *Comparison of the MSE curves for the modified VSSLMS algorithms with their original versions (SNR=10dB)*

Figure 6 clearly illustrates that the VSSLMS algorithm with modification of variable forgetting factor effectively enhances the convergence performance of the VSSLMS algorithms. For ease of representation, the modified version of these VSSLMS algorithms is abbreviated in this paper as MVSSLMS-A, MVSSLMS-B, MVSSLMS-C and MVSSLMS-D respectively. In the previous comparison of the convergence effects among the above VSSLMS algorithms, MVSSLMS-D algorithm consistently outperforms several other VSSLMS algorithms. Its comprehensive representation is presented in Equations (40) to (44).

$$\widehat{\boldsymbol{Q}}(t+1) = \widehat{\boldsymbol{Q}}(t)+\mu(t)e_{\hat{Q}}(t)\boldsymbol{\Phi}^{*}(t) \tag{40}$$

$$\mu(t) = \xi(t)\mu(t-1) + \eta(t)e_{\hat{Q}}^{2}(t-1) \tag{41}$$

$$\xi(t)=\lambda_1(0)+1-\lambda_1(t) \tag{42}$$

$$\lambda_1(t)=\lambda_0\lambda_1(t-1)+1-\lambda_0 \tag{43}$$

$$\eta(t) = \beta\cdot\operatorname{arccot}(\left|e_{\hat{Q}}(t)\right|) \tag{44}$$

When utilizing MVSSLMS-D as the PAA for the feedback AVC system, the operation of the entire feedback AVC controller can be summarized as follows:

Based on the system error $e_{\hat{Q}}(t)$ measured in the current control cycle and the controller output $u(t)$, the input signal $\omega(t)$ of the adaptive filter can be obtained according to equation (13).

The observation vectors $\boldsymbol{\Phi}(t)$ and $\boldsymbol{\Phi}^*(t)$ of the perturbed signals are constructed according to equation (27) and (28).

The adaptive filter parameter vector $\widehat{\boldsymbol{Q}}(t+1)$ is updated according to equation (40) to (44).

Calculate the controller output $u(t+1)$ for the next control cycle according to equation (35).

The stability characteristics and admissible parameter ranges of the proposed algorithm are summarized as follows. The stability of the proposed feedback adaptive control system is theoretically guaranteed by the Youla–Kučera (Y–K) parameterization framework. Because the adaptive filter is embedded in a closed-loop structure whose characteristic polynomial remains unchanged, the internal stability of the system is preserved. For the parameter adaptation governed by the VSSLMS algorithm, mean-square stability can be ensured when the step-size μ and the forgetting-factor λ satisfy $0 < \mu < 2/(\gamma P_{max})$and $0 < \lambda < 1$, where P_{max}denotes the maximum input-signal power and γ is an empirical safety margin. These bounds guarantee convergence of the adaptive law without causing oscillatory behavior. In practice, μ is selected in the range 0.001–0.05 and λ is initialized close to 1 (e.g., 0.98–0.995) to balance convergence speed and steady-state accuracy.

4 Experimental verification of micro-vibration active control

In this section, we utilize the micro-vibration active isolation experimental system established in the previous section to select a specific actuation direction for comparative verification of the SISO micro-vibration active control algorithm. During the experiments, various typical disturbance signal features are chosen as micro-vibration disturbance excitation sources based on a multi-frequency narrow-band disturbance environment. This is done to assess the vibration suppression performance of the proposed Y-K parameterization-based feedback vibration active control algorithm under different disturbance scenarios.

4.1 Dual-frequency sinusoidal perturbation

The micro-vibration excitation signal used is the superposition of two sinusoidal signals with frequencies of 10 Hz and 25 Hz. Figure 7 displays the time-domain effects of active control of micro-vibration under dual-frequency sinusoidal perturbation excitation. In Figure 7, the FxLMS adaptive control algorithm achieves a suppression efficiency of approximately 50% for the dual-frequency disturbance removal. In comparison to the adaptive control algorithm alone, the other two robust adaptive control algorithms based on the Y-K parameterization method exhibit significantly improved steady-state effects, with vibration at steady state measuring only 0.3 μm.

In the robust adaptive control algorithm based on the Y-K parameterization method, the parameter adaptive algorithm is chosen to be the LMS algorithm and the VSSLMS algorithm proposed in this paper, respectively. Through multiple parameter adjustments, it was observed that there is little difference in the vibration suppression effect between the LMS algorithm and the VSSLMS algorithm when used as the parameter adaptive algorithm under dual-frequency narrow-band disturbance excitation. For ease of representation, the three algorithms are abbreviated as FxLMS, Q+LMS, and Q+VSSLMS in the figure legends, and these abbreviations continue to be used in the subsequent sections.

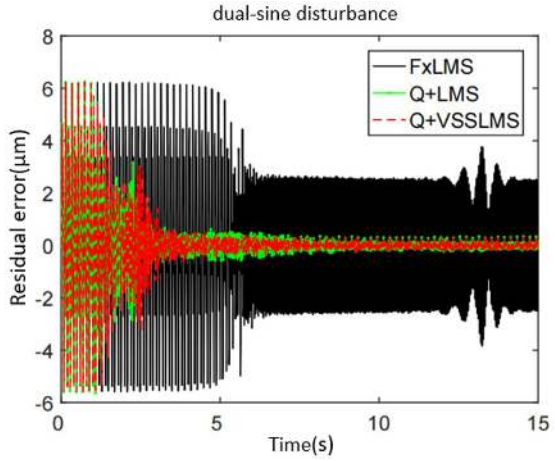

Figure 7 Control effect of AVC algorithms under a dual sine disturbance signal

Although the steady-state vibration amplitudes achieved by Q+LMS and Q+VSSLMS are similar, the convergence characteristics differ significantly. The Q+VSSLMS algorithm reaches steady-state within approximately 3.2 s, while

Q+LMS requires about 5.4 s under the same conditions. This faster convergence confirms that the variable step-size mechanism enhances the adaptation speed without compromising stability.

4.2 Spectrum mutation

In the spectrum mutation experiment, the amplitude remains unchanged while changing the frequency.Similar to the dual-frequency sinusoidal disturbance, the micro-vibration excitation signal is created by superimposing two sinusoidal signals with frequencies of 10 Hz and 25 Hz. During the 20-second experiment, the frequency of the perturbing signal abruptly changed to 11 Hz and 26 Hz. Figure 8 displays the time-domain curves of micro-vibration active control under the sudden change in frequency of the external disturbance excitation.

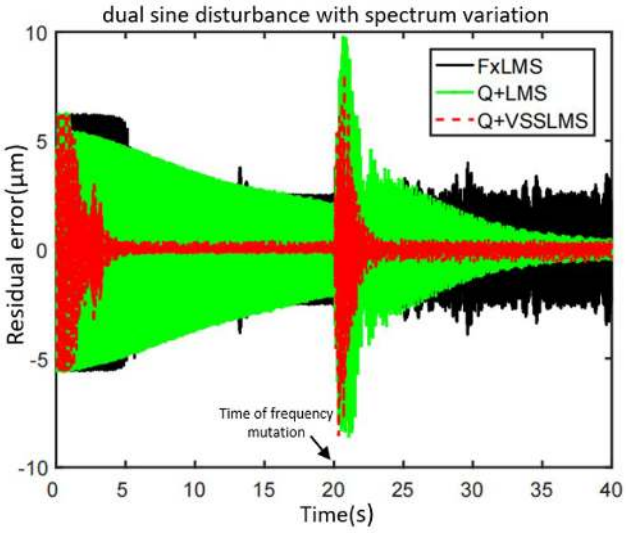

Figure 8 Control effect for AVC algorithms under a dual sine disturbance signal with frequency spectrum variation

4.3 Amplitude mutation

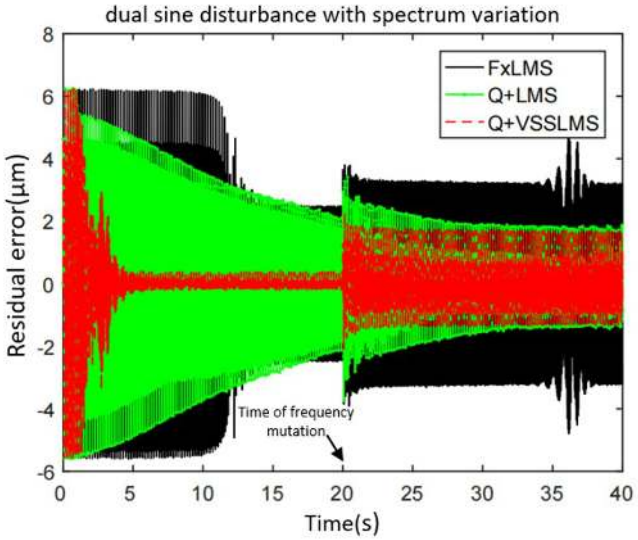

Figure 9 Control effect for AVC algorithms under a dual sine disturbance signal with amplitude variation

In line with the previous two experiments, we began with dual-frequency narrow-band sinusoidal perturbations at 10 Hz and 25 Hz. At the 20-second mark, the amplitude of each sinusoidal perturbation signal abruptly increased to 125%

of its original amplitude. Figure 8 illustrates the time-domain effects of micro-vibration active control under the abrupt amplitude perturbation excitation.

As shown in Figure 9, the vibration suppression effect of all three algorithms is diminished to varying degrees following the amplitude mutation. The steady-state amplitude of the Q+VSSLMS algorithm changes from 0.3μm before the mutation to 1.5μm after the mutation, but it remains superior to the Q+LMS and FxLMS algorithms.

Based on the experiments involving the active control of micro-vibrations under three typical disturbance excitations, the following observations can be made:

1) Under dual-frequency sinusoidal narrow-band disturbances, the robust adaptive control algorithm based on the Y-K parameterization method significantly outperforms the FxLMS adaptive control algorithm in terms of vibration suppression.

2) The Q+VSSLMS algorithm achieves more satisfactory results when dealing with spectrum mutations and amplitude mutations in dual-frequency sinusoidal narrow-band perturbations. Compared to the Q+LMS algorithm, the VSSLM algorithm designed in this paper can adjust the step factor of the parameter adaptive algorithm in real-time, enabling the algorithm to quickly converge to the new steady state under the new perturbation and exhibit improved robustness.

The robustness of the proposed feedback adaptive controller can be theoretically explained by the Y–K parameterization framework, in which the inclusion of the adaptive filter $Q(z)$ does not alter the closed-loop poles defined by the central robust controller $C(z)$. This structural invariance ensures that the system stability is preserved even when the secondary path model is uncertain or time-varying.

The experimental observations in Figures 7–9 directly reflect this property. When the disturbance spectra or amplitudes change abruptly, the FxLMS and Q+LMS algorithms exhibit transient instability and slower re-convergence, whereas the proposed Q+VSSLMS algorithm maintains bounded error dynamics and rapidly restores steady-state performance. This behavior confirms the theoretical prediction that the adaptive law enhances disturbance rejection while maintaining closed-loop robustness guaranteed by the Y–K formulation.

The proposed feedback adaptive controller can also be extended to vibration scenarios with more frequency components. Since the Y–K parameterization framework ensures structural stability, adding additional adaptive filter taps increases the controller's ability to represent multiple narrow-band disturbance frequencies simultaneously. The VSSLMS update mechanism automatically distributes adaptation among these components according to the instantaneous vibration energy. As the number of disturbance frequencies increases, convergence speed may decrease slightly due to higher filter dimensionality; however, stability and steady-state accuracy are maintained as long as the step-size and forgetting-factor parameters remain within their admissible ranges. This scalability demonstrates that the proposed algorithm is suitable for complex multi-frequency vibration environments.

5 Conclusions

In this paper, we introduce a feedback adaptive vibration active control algorithm and a novel VSSLMS parameter adaptive algorithm based on the Y-K parameterization method. Our objective is to achieve micro-vibration control of satellite structures under multi-frequency unknown and time-varying narrow-band disturbances, especially when the secondary channel model is unknown.

The advantages of the VSSLMS algorithm proposed in this paper are validated through system identification simulations. Additionally, the robustness of the Y-K parameterization-based feedback robust adaptive control algorithm is demonstrated in comparison to other algorithms in scenarios involving sudden changes in the amplitude of disturbance signal spectra, as confirmed by real-time micro-vibration control experiments.

Author's Contribuitions: Conceptualization, Yubin Fang and Mengchu Tian; Methodology, Yubin Fang; Investigation, Chaojun Liang, Yubin Fang; Writing - original draft, Yubin Fang, Chaojun Liang and Mengchu Tian; Writing - review & editing, Mengchu Tian; Funding acquisition, Yubin Fang and Mengchu Tian; Resources, Yubin Fang, Chaojun Liang, and Mengchu Tian.

Data Availability: Research data is only available upon request

Editor: Rogério José Marczak

References

[1] LEE D-O, PARK G, HAN J-H. (2016). Hybrid isolation of micro vibrations induced by reaction wheels[J]. *Journal of Sound and Vibration*, 363: 1-17.

[2] LI L, YUAN L, WANG L, et al. (2021). Recent advances in precision measurement & pointing control of spacecraft[J]. *Chinese Journal of Aeronautics*, 34(10): 191-209.

[3] MENG G, ZHOU X. (2015). Progress review of satellite micro-vibration and control[J]. *Acta Aeronautica et Astronautica Sinica*, 36(8): 2609-2619.

[4] WANG L, LIU J, LI Y. (2020). The optimal controller design framework for PID-based vibration active control systems via non-probabilistic time-dependent reliability measure[J]. *Isa Transactions*, 105: 129-145.

[5] SUN Y, LI C, CHANG Y, et al. (2018). Finite-time vibration control of space intelligent truss[J]. *Journal of Harbin Institute of Technology*, 50(10): 27-34.

[6] LANDAU I D. (2020). On the use of Youla–Kucera parametrization in adaptive active noise and vibration control – a review[J]. *International Journal of Control*, 93(2): 204-216.

[7] WANG J, ARANOVSKIY S V, BOBTSOV A A, et al. (2017). Compensating for a Mult sinusoidal disturbance based on Youla-Kucera parametrization[J]. *Automation and Remote Control*, 78(9): 1559-1571.

[8] YOULA D, BONGIORNO J, JABR H. (1976a). Modern Wiener--Hopf design of optimal controllers Part I: The single-input-output case[J]. *IEEE Transactions on Automatic Control*, 21(1): 3-13.

[9] YOULA D, JABR H, BONGIORNO J. (1976b). Modern Wiener-Hopf design of optimal controllers--Part II: The multivariable case[J]. *IEEE Transactions on Automatic Control*, 21(3): 319-338.

[10] ANDERSON B D O. (1998). From Youla–Kucera to Identification, Adaptive and Nonlinear Control[J]. *Automatica*, 34(12): 1485-1506.

[11] LANDAU I D, ALMA M. (2010). An adaptive feedforward compensation algorithm for active vibration control[C], *49th IEEE Conference on Decision and Control (CDC)*, Atlanta, GA, USA, pp: 3626-3631, doi: 10.1109/CDC.2010.5717646.

[12] LANDAU I D, AIRIMITOAIE T B, ALMA M. (2011a). A Youla-Kucera parametrized adaptive feedforward compensator for active vibration control[J]. *18th IFAC Proceeding Volumes*, 44(1): 3427-3432.

[13] LANDAU I D, AIRIMIŢOAIE T B, ALMA M. (2012). An IIR Youla-Kucera parametrized adaptive feedforward compensator for active vibration control with mechanical coupling[J]. *IEEE Transactions on Control Systems Technology*, 48(9): 2152-2158.

[14] LANDAU I D, AIRIMIŢOAIE T B, ALMA M. (2013). IIR Youla–Kucera Parameterized Adaptive Feedforward Compensators for Active Vibration Control With Mechanical Coupling[J]. *IEEE Transactions on Control Systems Technology*, 21(3): 765-779.

[15] TUDOR-BOGDAN AIRIMITOAIE I D L, RAUL MELENDEZ, LUC DUGARD. (2013). Algorithms for Adaptive Feedforward Noise Attenuation–A Unified Approach and Experimental Evaluation[J]. *IEEE Transactions on Control Systems Technology*, 29(5): 1850-1862.

[16] LANDAU I D, AIRIMITOAIE T B, MELENDEZ R, et al. (2019a). Why one should use Youla-Kucera parametrization in adaptive feedforward noise attenuation[C], *58th Conference on Decision and Control (CDC)*, Nice, France, pp: 78-83, doi: 10.1109/CDC40024.2019.9029440.

[17] LANDAU I D, MELENDEZ R, AIRIMITOAIE T B, et al. (2019b). Beyond the delay barrier in adaptive feedforward active noise control using Youla-Kucera parametrization[J]. *Journal of Sound and Vibration*, 455: 339-358.

[18] AIRIMITOAIE T B, LANDAU I D, MELENDEZ R, et al. (2021). Algorithms for Adaptive Feedforward Noise Attenuation-A Unified Approach and Experimental Evaluation[J]. *IEEE Transactions on Control Systems Technology*, 29(5): 1850-1862.

[19] LANDAU I D, ALMA M, MARTINEZ J J, et al. (2011b). Adaptive Suppression of Multiple Time-Varying Unknown Vibrations Using an Inertial Actuator[J]. *IEEE Transactions on Control Systems Technology*, 19(6): 1327-1338.

[20] SILVA A C, LANDAU I D, AIRIMITOAIE T-B. (2013). Direct adaptive rejection of unknown time-varying narrow band disturbances applied to a benchmark problem[J]. *European Journal of Control*, 19(4): 326-336.

[21] LANDAU I D, AIRIMITOAOE T B, CASTELLANOS SILVA, et al. (2016). Adaptive and Robust Active Vibration Control—methodology and Tests, Advances in Industrial Control[M]. London: Springer.

[22] CHEN X, JIANG T Y, TOMIZUKA M. (2015). Pseudo Youla-Kucera parameterization with control of the waterbed effect for local loop shaping[J]. *Automatica*, 62: 177-183.

[23] LANDAU I D, AIRIMITOAIE T B, SILVA A C. (2015). Adaptive attenuation of unknown and time-varying narrow band and broadband disturbances[J]. *International Journal of Adaptive Control and Signal Processing*, 29(11): 1367-1390.

[24] VAU B, LANDAU I D. (2021). Adaptive rejection of narrow-band disturbances in the presence of plant uncertainties-A dual Youla-Kucera approach[J]. *Automatica*, 129: 109618.

[25] AIRIMITOAIE T-B, LANDAU I D. (2018). Combined adaptive feedback and feedforward compensation for active vibration control using Youla–Kučera parametrization[J]. *Journal of Sound & Vibration*, 434: 422-441.

[26] QIAN F F, WU Z Z, ZHANG M T, et al. (2019). Youla parameterized adaptive vibration control against deterministic and band-limited random signals[J]. *Mechanical Systems and Signal Processing*, 134: 106359.

[27] WU Z, ZHANG M, CHEN Z, et al. (2019). Youla parameterized adaptive vibration suppression with adaptive notch filter for unknown multiple narrow band disturbances[J]. *Journal of Vibration and Control*, 25(3): 685-694.

[28] KWONG R H, JOHNSTON E W. (1992). A variable step size LMS algorithm[J]. *IEEE Transactions on Signal Processing*, 40(7): 1633-1642.

[29] ABOULNASR T, MAYYAS K. (1995). A robust variable step-size LMS-type algorithm: analysis and simulations[J]. *IEEE Transactions on Signal Processing*, 45(3): 631-639.

[30] HUANG B, XIAO Y, MA Y, et al. (2015). A simplified variable step-size LMS algorithm for Fourier analysis and its statistical properties[J]. *Signal Processing*, 117: 69-81.

[31] FANG Y B, ZHU X J, GAO Z Y, et al. (2019). New feedforward filtered-x least mean square algorithm with variable step size for active vibration control[J]. *Journal of Low Frequency Noise Vibration and Active Control*, 38(1): 187-198.

[32] Ruan Y, Xu T, Tang T, Peng Z. (2022). Adaptive Youla–Kučera parametric control of unknown tip-tilt disturbance rejection in image stabilization systems [J]. Optics Letters, 47(10): 2670-2673.

[33] Ding H, Li F, Qian F, et al. (2024). LQG/LTR based robust Youla parameterized adaptive vibration control for the supporting platform of rotating liquid mirror [J]. Journal of Vibration and Control, 31(3-4): 284-300.

[34] Ruan Y, Xu T, Tang T, Peng Z. (2024). Vibration control of a flexible inverted pendulum using the planned flywheel motion [J]. Journal of Sound and Vibration, 569: 117975.

[35] Zhang L, Huang Z, Ma H. (2024). Three-dimensional vibration suppression of flexible beams via flywheel assembly [J]. Mechanics & Industry, 25(4): 105-118.

[36] Chu W, Wang Y Q. (2025). A novel method for suppressing oscillations of suspended loads [J]. Ocean Engineering, 342: 122839.